



**HAL**  
open science

# **An idealized two-dimensional approach to study the impact of the West African monsoon on the meridional gradient of tropospheric ozone**

M. Saunois, C. Mari, V. Thouret, Jean-Pierre Cammas, P. Peyrillé, J.P. Lafore, B. Sauvage, A. Volz-Thomas, P. Nédélec, Jean-Pierre Pinty

## ► To cite this version:

M. Saunois, C. Mari, V. Thouret, Jean-Pierre Cammas, P. Peyrillé, et al.. An idealized two-dimensional approach to study the impact of the West African monsoon on the meridional gradient of tropospheric ozone. *Journal of Geophysical Research: Atmospheres*, 2008, 113 (D07), pp.D07306. 10.1029/2007JD008707 . hal-00282388

**HAL Id: hal-00282388**

**<https://hal.science/hal-00282388>**

Submitted on 29 Jul 2021

**HAL** is a multi-disciplinary open access archive for the deposit and dissemination of scientific research documents, whether they are published or not. The documents may come from teaching and research institutions in France or abroad, or from public or private research centers.

L'archive ouverte pluridisciplinaire **HAL**, est destinée au dépôt et à la diffusion de documents scientifiques de niveau recherche, publiés ou non, émanant des établissements d'enseignement et de recherche français ou étrangers, des laboratoires publics ou privés.

Copyright

## An idealized two-dimensional approach to study the impact of the West African monsoon on the meridional gradient of tropospheric ozone

M. Saunois,<sup>1,2</sup> C. Mari,<sup>1,2</sup> V. Thouret,<sup>1,2</sup> J. P. Cammas,<sup>1,2</sup> P. Peyrillé,<sup>3</sup> J. P. Lafore,<sup>3</sup> B. Sauvage,<sup>1,2</sup> A. Volz-Thomas,<sup>4</sup> P. Nédélec,<sup>1,2</sup> and J. P. Pinty<sup>1,2</sup>

Received 27 March 2007; revised 16 October 2012; accepted 11 December 2007; published 10 April 2008.

[1] An idealized vertical-meridional zonally symmetrical version of the Méso-NH model is used to study the response of tropospheric ozone to the dynamics of the West African monsoon, as well as surface emissions and NO<sub>x</sub>-production by lightning (LNO<sub>x</sub>). An O<sub>3</sub>-NO<sub>x</sub>-VOC chemical scheme has been added to the dynamical model, including surface emissions and a parameterization of the LNO<sub>x</sub> production. The model shows that the ozone precursors emitted at the surface are uplifted by deep convection and then advected in the upper branches of the Hadley cells on both sides of the Inter Tropical Convergence Zone (ITCZ). The NO<sub>x</sub> produced by lightning promotes chemical ozone production in the middle and upper troposphere from the oxidation of CO and VOCs. The analysis of the convective and chemical tendencies shows that the ozone minimum at the ITCZ is induced by venting of ozone-poor air masses into the upper troposphere. The bi-dimensional model suffers from limitations due to the absence of exchange with the higher latitudes and ventilation in the zonal direction. Despite of these restrictions, sensitivity simulations show that the LNO<sub>x</sub> source and biogenic VOCs are necessary to create the meridional gradient of ozone observed by the Measurements of Ozone and water vapor by in-service Airbus airCraft (MOZAIC) aircrafts in the southern Hadley cell. The LNO<sub>x</sub> source is also required to maintain the meridional ozone gradient up to 24°N in the northern Hadley cell. The modeled meridional gradient of O<sub>3</sub> in the upper troposphere ranges from 0.22 to 0.52 ppbv/deg without the LNO<sub>x</sub> source and from 0.60 to 1.08 ppbv/deg with the LNO<sub>x</sub> source, in the southern and the northern cells respectively.

**Citation:** Saunois, M., C. Mari, V. Thouret, J. P. Cammas, P. Peyrillé, J. P. Lafore, B. Sauvage, A. Volz-Thomas, P. Nédélec, and J. P. Pinty (2008), An idealized two-dimensional approach to study the impact of the West African monsoon on the meridional gradient of tropospheric ozone, *J. Geophys. Res.*, 113, D07306, doi:10.1029/2007JD008707.

### 1. Introduction

[2] Tropospheric ozone plays an important role in the oxidation capacity of the global atmosphere. High UV radiation and humidity promote the formation of OH from photolysis of O<sub>3</sub> [Thompson, 1992]. Ozone is produced in the troposphere by photochemical oxidation of CO and hydrocarbons in presence of nitrogen oxides (NO<sub>x</sub> = NO + NO<sub>2</sub>). Over Africa, biomass burning during the dry season leads to large emissions of CO, hydrocarbons and nitrogen oxides over Africa. In July, the burning occurs preferentially in the southern hemisphere [Jonquière *et al.*, 1998; Sauvage

*et al.*, 2005; Edwards *et al.*, 2006]. In addition, ozone precursors are emitted from soils and vegetation, particularly between 5°N and 15°N over West Africa [Guenther *et al.*, 1995, 2006; Serça *et al.*, 1998; Jaeglé *et al.*, 2004, 2005] and from industrialized areas, especially in Nigeria [Olivier *et al.*, 2003]. Moreover, the electrical activity associated with deep convection systems at the Inter Tropical Convergence Zone (ITCZ) [Christian *et al.*, 2003] is a major source of NO in the upper tropical troposphere [Pickering *et al.*, 1996; Bond *et al.*, 2002; Labrador *et al.*, 2005; Martin *et al.*, 2007; Sauvage *et al.*, 2007a]. It was shown that lightning produced NO<sub>x</sub> is of great influence on the ozone distribution in the middle and upper troposphere [e.g., Martin *et al.*, 2000; DeCaria *et al.*, 2005]. Only a few studies have been devoted to the understanding of the ozone budget over Africa during the wet season. Recently, Aghedo *et al.* [2007] have investigated the influence of these different sources on the ozone burden with a global 3D model. The authors emphasize the role of biogenic emissions on the ozone budget over Africa. Lightning leads to the second largest impact on the middle and upper tropospheric ozone concentration. Despite of these new results,

<sup>1</sup>Université de Toulouse, Laboratoire d'Aérodynamique, Toulouse, France.

<sup>2</sup>Centre National de la Recherche Scientifique, UMR5560, Toulouse, France.

<sup>3</sup>Centre National de Recherches Météorologiques, Toulouse, France.

<sup>4</sup>Institut für Chemie und Dynamik der Geosphäre II: Troposphäre, Forschungszentrum Jülich, Jülich, Germany.

the understanding of meteorological and chemical processes in this region is weak. The relative contributions of the different sources and their redistribution at the global scale are still not well known.

[3] Over West Africa the lack of in situ observations makes the study of the ozone budget difficult. The MOZAIC (Measurements of OZone and water vapor by in-service Airbus airCraft) program provides a unique and extensive source of data over Africa for ozone, water vapor and carbon monoxide, as well as data for total odd nitrogen ( $\text{NO}_y$ ). Recently, *Sauvage et al.* [2007b] using MOZAIC data between 1994 and 2004 showed an ozone minimum collocated with a relative humidity maximum at the ITCZ and a meridional ozone gradient of  $0.94 \pm 0.18$  ppbv/deg between  $12^\circ\text{N}$  and  $30^\circ\text{N}$  during boreal summer (JJA). They suggested that both convective transport of poor ozone air masses and photochemical ozone production in the upper level branches of the Hadley cells could contribute to these gradients.

[4] The aim of this study is to understand how this gradient is induced by the meridional circulation of the Hadley cells and to assess the relative contributions of convective transport and photochemistry production on one hand and the relative contributions of the surface sources and the lightning source on the other hand.

[5] For this purpose, a model is required that covers the scales and the processes relevant for the dynamics of the West African monsoon (henceforth denoted WAM), which are driven by ocean-atmosphere-land coupling [*Zeng et al.*, 1999; *Giannini et al.*, 2003]. The spatial and temporal scales involved range from global circulation to local convection and many processes (convection, evaporation, turbulence) interact [*Rowell et al.*, 1995; *Redelsperger et al.*, 2002]. Global circulation models, albeit taking into account the entire complexity of the system, generally fail to produce a realistic WAM. Several studies have shown that dynamical models are not accurate enough in West Africa regions and are unable to simulate fundamental characteristics of rainfall (diurnal, seasonal and annual cycles) [*Thiaw and Mo*, 2005; *Pinker et al.*, 2006; *Douville et al.*, 2007]. To better understand the interactions of scales and processes of the WAM at these low spatial resolutions, a complementary approach is to use a model of intermediate complexity in which the main interactions are more easily quantifiable than in a complete GCM. This methodology has been used in several studies concerning, e.g., the sensitivity of the WAM to the distribution of the moist static energy [*Eltahir and Gong*, 1996; *Zheng et al.*, 1999; *Wang and Eltahir*, 2000] or the influence of Rossby waves [*Chou et al.*, 2001]. *Peyrillé et al.* [2007] studied the WAM with an idealized model describing a vertical meridional cross section. This simplification is justified because of the zonal symmetry between  $10^\circ\text{W}$  and  $10^\circ\text{E}$  of many parameters, such as vegetation cover, surface temperature and albedo. They used the meso-scale model of the French community Méso-NH [*Lafore et al.*, 1998] including a complete physical package to build the 2-dimensional model. The idealized model of *Peyrillé et al.* [2007] recovers the typical July monsoon regime quite well and can hence be used in a chemistry framework to study the distribution of ozone and its precursors over West Africa.

## 2. MOZAIC Data

[6] The MOZAIC program (<http://mozaic.aero.obs-mip.fr>) has provided regular measurements of ozone and water vapor from 5 long-haul aircraft since 1994 [*Marenco et al.*, 1998; *Thouret et al.*, 1998a, 1998b]. Ozone is measured by a dual beam UV-absorption instrument (Thermo Instruments) with an overall precision of  $\pm[2 \text{ ppbv} + 2\%]$ . For water vapor, a special airborne humidity sensing device (AD-FS2), developed by Aerodata (Braunschweig, Germany) and based on the humidity and temperature transmitter HMP 230 of Vaisala (Helsinki, Finland), is used for measuring relative humidity and temperature of the atmosphere. Regular laboratory calibrations have shown that the uncertainty on the measurements of relative humidity ranges from 4% in the midtroposphere to 7% in the UT between 9 and 13 km altitude [*Helten et al.*, 1998]. Since 2001, CO measurements are also performed aboard the MOZAIC aircrafts and one aircraft is equipped to sample  $\text{NO}_y$  [*Volz-Thomas et al.*, 2005; *Pätz et al.*, 2006]. Since 1997, MOZAIC flights between Europe and Africa are available, providing a unique data set for Equatorial Africa [*Sauvage et al.*, 2005]. In the paper, we use all data from flights between Europe and 14 airports of cities over West Africa. The flight tracks are quasi meridional transects. The data were combined to provide average meridional profiles of ozone, water vapor and winds between  $10^\circ\text{W}$  and  $20^\circ\text{E}$  for the summer months (JJA) of the 1994–2004 period. The measurements at cruise altitude were filtered with a threshold of 100 ppbv  $\text{O}_3$  to exclude stratospheric intrusions [*Thouret et al.*, 1998b]. Unfortunately the flights providing CO and  $\text{NO}_y$  measurements are too sparse in the studied period 1994–2004 over West Africa to derive a representative latitudinal distribution for these species. In this paper we only analyze the seasonal mean for boreal summer (JJA) but the behavior discussed below is also reproduced during the boreal winter season.

[7] The seasonal mean for JJA is shown in Figure 1. The maximum in relative humidity (55% RH) at  $7^\circ\text{N}$  identifies the location of the ITCZ and the descending branch of the Hadley cells at  $25\text{--}30^\circ\text{N}$  is identified by a minimum in RH. The zonal wind shows the presence of the Tropical Easterly Jet at  $4^\circ\text{N}$  and the Subtropical Westerly Jet north of  $30^\circ\text{N}$ . The meridional wind generally changes its direction around the location of the maximum RH-values. This feature is in line with the average Hadley circulation. The dynamical characteristics of the West African upper troposphere are well sampled by the MOZAIC measurements. The MOZAIC measurements show minimum values of ozone around 45 ppbv in the upper troposphere which are collocated with the maximum of RH at the ITCZ. A pronounced gradient of ozone is observed between the ITCZ and the Saharan desert. A linear regression gives an ozone gradient of  $1.13 \pm 0.17$  ppbv/deg between  $7^\circ\text{N}$  and  $32^\circ\text{N}$ , slightly larger than the gradient of  $0.94 \pm 0.18$  ppbv/deg described by *Sauvage et al.* [2007b] for the region between  $12^\circ\text{N}$  and  $30^\circ\text{N}$  and  $5^\circ\text{W}$  and  $30^\circ\text{E}$ .

## 3. Model Description

[8] For our study, we used the 2-dimensional model described by *Peyrillé et al.* [2007] and built to identify

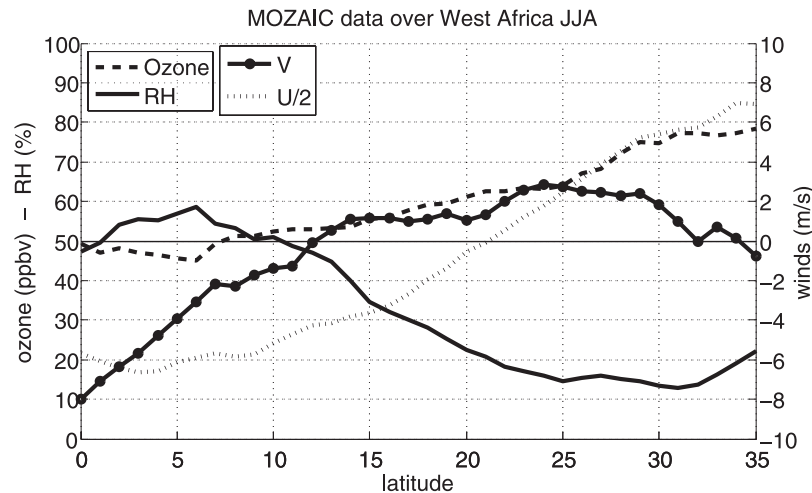


**Figure 1.** Upper tropospheric (9–12 km) meridional profiles observed by MOZAIC in JJA for ozone mixing ratio (ppbv), relative humidity (%) and zonal and meridional winds (m/s) between 0°N and 35°N.

the key factors that control the WAM. This idealized model is based on the French community atmospheric simulation system Méso-NH [Lafore *et al.*, 1998], and represents the average atmospheric circulation between 10°W and 10°E.

[9] Briefly, the 2-D model of Peyrillé *et al.* [2007] extends from 30°S to 40°N with a horizontal resolution of 70 km. The vertical domain extends to 20 km, with a stretched grid of 30 m near the surface to 1 km in the upper troposphere. A so-called sponge layer above 20 km is implemented as upper boundary in order to prevent wave-reflection at the top. Rigid wall boundary conditions are imposed so that neither mass (of chemical species in particular) nor energy exchanges are allowed to occur between the model domain and the higher latitudes. The West African subcontinent is approximated as a flat continental band between 5°N and 30°N. Orographically induced circulation is hence not considered. Peyrillé *et al.* [2007] have shown that adding a plateau induces a northward displacement of the monsoon of about 3°. The parametrization of convection is adopted from Bechtold *et al.* [2001], including transport and scavenging of soluble species [Mari *et al.*, 2000]. HNO<sub>3</sub> is scavenged by liquid precipitation and captured by ice in the convective columns. The ice uptake of HNO<sub>3</sub> out of the convective column (e.g., cirrus) is not considered in this work. A sensitivity simulation with a complete uptake of HNO<sub>3</sub> by resolved ice in the model shows dramatic changes of HNO<sub>3</sub> distribution but low effect on the ozone concentrations (less than 3 ppbv) in the upper troposphere in agreement with von Kuhlmann and Lawrence [2006]. Turbulent processes are represented by the one-dimensional version of the turbulent scheme of Cuxart *et al.* [2000], based on the mixing length of Bougeault and Lacarrère [1989] and including a prognostical turbulent energy equation. Sea surface temperature (Atlantic Ocean and Mediterranean Sea) are taken from the Reynolds climatology of 1982–2003 [Reynolds and Smith, 1995] using July profiles for the Gulf of Guinea and May profiles for the Mediterranean Sea. The role of the SSTs in the Mediterranean Sea has been pointed out by Peyrillé *et al.* [2007]. The Mediterranean Sea warming between May and July decreases the thermal contrast with the continent and

increases the humidification of the Sahara. Both effects favor a northward penetration of the WAM. In addition, the absence of zonal advection in the idealized 2D model leads to an underestimation of the warming and drying in the Sahara region at low levels. In a companion paper, Peyrillé and Lafore [2007] have parameterized the effects of the third dimension by adding an advective forcing for temperature and humidity. These forcings are not accounted in the present version of the model but their effects are in fact compensated here with a colder SST in Mediterranean Sea. The flux parametrization over the ocean for tropical winds is implemented according to Mondon and Redelsperger [1998]. The exchange between surface and atmosphere is described by the ISBA scheme of Mahfouf and Noilhan [1996].

[10] For the present study, the model of Peyrillé *et al.* [2007] was completed with the chemistry solver ReLACS (Regional Lumped Atmospheric Chemical Scheme, Crassier *et al.* [2000]), which is based upon a reduction of the Regional Atmospheric Chemistry Mechanism (RACM) [Stockwell *et al.*, 1997]. ReLACS considers 37 chemical species and 128 equations. This chemical scheme is suitable for the simulation of clean and polluted atmospheres.

[11] Surface emissions fluxes were taken from the POET/GEIA inventory and represent the average emissions fluxes over the longitudinal band 10°W–10°E (Table 1). The latitudinal gradient of the surface emissions was kept constant throughout the simulation except for the VOCs emissions from vegetation for which a diurnal cycle is considered. Natural emissions from vegetation of CO and VOCs were taken into account between 5°N and 15°N. It is worth noting that NO<sub>x</sub> emissions from soils are forced constant in time. A latitudinal gradient of the NO<sub>x</sub> emissions from soils is considered at 10°N to distinguish areas with thick vegetation cover and areas with vegetation and bare soils. In the real world, these emissions have significant temporal (on intraseasonal and daily basis) and geographical variabilities which are not taken into account in the model. Despite of this oversimplification, the simulated NO<sub>x</sub> in the boundary layer are in the range of aircraft observed values between 100 and 700 pptv (C. Reeves,

**Table 1.** Surface and Lightning Emissions in Mg(N)/Month for NO<sub>x</sub> and in Mg(C)/Month for CO and Hydrocarbons<sup>a</sup> Emitted in the 2D Model. Surface Emissions are Adapted from the GEIA Database (See Text for Details)

Source	Geographical Location	NO <sub>x</sub>	CO	BIO	ETH	ALKA	ALKE	KET
Soils	5°N–10°N	400	...	...	...	...	...	...
	10°N–15°N	1000	...	...	...	...	...	...
Lightning	30°S–40°N	25	...	...	...	...	...	...
Ocean	(5°N & ) 15°N	...	620	...	84	55	210	...
Vegetation	5°N–15°N	...	11000	46000	150	1300	480	4

<sup>a</sup>BIO, ETH, ALKA, ALKE, and KET are the ReLACS (lumped) species for isoprene and monoterpene, ethane, alkane, alkene and ketone respectively [see *Crassier et al.*, 2000].

personal communication). Natural emissions of CO, ethane, alkanes and alkenes over the Atlantic Ocean and the Mediterranean Sea were also considered. Anthropogenic emissions were not considered in this study due to the large uncertainty in the inventory for West Africa. It is noted however, that adding a latitudinal dependent anthropogenic source to the model increases the mixing ratios of the precursors without significant influence on the ozone gradient in the upper troposphere.

[12] A parametrization of the NO<sub>x</sub> production by lightning (LNO<sub>x</sub>) has been implemented into the deep convection scheme by *Mari et al.* [2006]. The parametrization of the lightning frequency is based on *Price and Rind* [1992] and related to the convective cell height. The ratio IC/CG (IC stands for IntraCloud and CG for Cloud-to-Ground lightning) is derived from *Price and Rind* [1993] and depends on the depth of ice layers in the cloud. The NO production in the flashes is assumed to be proportional to air density along the flash. The specificity of this scheme is that it uses updraft and downdraft mass fluxes modeled by the deep convection scheme to generate the profile of lightning NO<sub>x</sub>. In the 2D model of the WAM, simulated flash rates range between 5 and 20 fl/min. The lightning detection network based in Benin in summer 2006 measured between 10 to 16 strokes/min for the IC contributions during one particular event (H. Höller, personal communication). Assuming that on average the number of flashes is half the number of strokes and that in the active phase there are about equal numbers of IC and CG strokes, the range of detected flash rates would range between 10 and 16 fl/min. The modeled flash rates are therefore in reasonable agreement with the few observations available over West Africa. By construction, the convection is triggered everyday at the same location. Consequently, a large source of NO<sub>x</sub> due to the lightning occurs at high frequency directly in the simulated upper troposphere. The wall boundary conditions in the north-south direction and the cyclic conditions in the east-west direction prevent this large amount of additional material to be ventilated correctly in the model. The LNO<sub>x</sub> source was therefore calibrated to 25 Mg(N)/month to obtain simulated ozone and NO<sub>y</sub> mixing ratios in agreement with the measurements made on board the MOZAIC aircrafts.

[13] Deposition velocities for O<sub>3</sub>, NO, NO<sub>2</sub>, HNO<sub>3</sub> and H<sub>2</sub>O<sub>2</sub> were adopted from *Seinfeld and Pandis* [1998] and for HCHO, aldehydes and PAN from *von Kuhlmann et al.* [2003].

[14] The model was initialized with a quiet, horizontally homogeneous, and almost dry (10% relative humidity) atmosphere. For initialization, the mixing ratios of the chemical species have been put constant (50 ppbv for O<sub>3</sub>,

100 ppbv for CO, 10 pptv for NO and NO<sub>2</sub> and 1 pptv the others species), and the influence of the initial values is found negligible after 25 days of simulation. The model was then integrated for 30 days, with solar conditions corresponding to 15th July including diurnal variation.

## 4. Results

### 4.1. Dynamics

[15] In this paragraph the main results found by *Peyrillé et al.* [2007] are summarized to highlight the dynamical behavior of the model.

[16] Starting from a quiet atmosphere, *Peyrillé et al.* [2007] have shown that 10 to 15 days spin-up are needed for the system to develop a deep convection zone. After 15 days the monsoon regime is fully established and in good agreement with the ERA-40 reanalysis of the European Center for Medium-Range Weather Forecast (ECMWF) [*Simmons and Gibson*, 2000]. However, the system is not steady: an intense diurnal cycle of the potential temperature and a northward drift of the system are observed [see *Peyrillé et al.*, 2007, Figure 3]. This induces a northward drift of the ITCZ, especially at the end of the simulation. Snapshots of the vertical-meridional cross sections of the meridional and zonal winds and the vertical velocities obtained for the 26th day at 1200UTC are shown in Figure 2. In the 2D model, the zonal wind is computed from the Coriolis effect on the meridional wind and from the meridional and vertical dissipation and advection. Similar to the results of *Peyrillé et al.* [2007], Figure 2 clearly exhibits the main features of the WAM, notably the deep convection zone around 10–15°N with ascents and secondary descents, the monsoon and Harmattan fluxes at the surface, as well as the African Easterly Jet around 5 km, the Tropical Easterly Jet and the SubTropical Jet near 12 km. The comparison with the ERA-40 reanalysis made by *Peyrillé et al.* [2007] shows that the jets derived from the 2D approach are stronger and shifted to the south (see their Figures 4 and 5). The meridional wind is quite realistic south to 20°N. The northerly branch corresponding to the winter cell is more intense but at higher latitude the model fails to recover well the indirect Hadley branch (see their Figures 4b and 5b). Compared to the ERA-40 reanalysis, the vertical velocities located at the ITCZ are too strong by a factor of 2. Subsidence is well reproduced in the free troposphere, except for too little subsidence over the Heat Low, (see their Figures 4c and 5c). The ascent simulated at 6°S over the ocean is somewhat questionable, and probably induced by the prescribed SSTs that create too much heat fluxes over the ocean. It corresponds to a rainy band in the

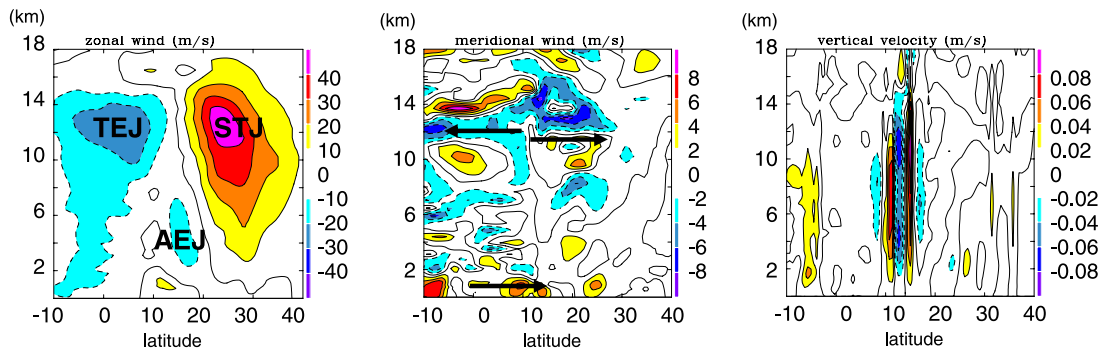


**Figure 2.** Vertical cross sections calculated for the 26th day of simulation at 1200 UTC: zonal and meridional winds and vertical velocity between  $-10^{\circ}\text{S}$  and  $40^{\circ}\text{N}$ . The three main jets over West Africa are highlighted: the African Easterly Jet (AEJ), the Tropical Easterly Jet (TEJ) and the SubTropical Jet (STJ).

simulation, but this is not observed in the data of the Global Precipitation Climatology Project for July.

**4.2. Sources of  $\text{CO}$ ,  $\text{NO}_x$  and  $\text{O}_3$  in the Upper Troposphere Over West Africa**

[17] Four simulations are considered in this study to assess the sensitivity of the meridional gradient of ozone to the chemical sources. The two principal simulations discussed in this section include the surface natural emissions with or without lightning emissions (thereafter LNOx and noLNOx respectively). Additional simulations (with or without some surface emissions) are discussed in section 6.

[18] It takes 10–15 days for the WAM model to reach a typical monsoon regime. After 25 days, the ozone distribution shows little day-to-day variations (not shown). The cross-sections in Figure 3 are obtained the 26th day of

simulation at 1200UTC: the results presented here are snapshots but nevertheless representative of a typical pattern of the simulated atmosphere.

[19] The  $\text{CO}$  and  $\text{NO}_x$  mixing ratios for the noLNOx case (top) in Figure 3 clearly show the convective transport at the ITCZ and the meridional transport by the Hadley cells. The  $\text{NO}_x$  mixing ratio presents a maximum of  $\sim 0.1$  ppbv around 14 km altitude. The  $\text{O}_3$  mixing ratio in the mid-troposphere is around 30–50 ppbv for the noLNOx case. Small areas of low ozone are found above intense ascending zones (around  $10^{\circ}\text{N}$  -ITCZ-,  $25^{\circ}\text{N}$  -Heat Low- and  $6^{\circ}\text{S}$  -over ocean-) which are the signatures of the venting of boundary layer air masses by convection. Around  $25^{\circ}\text{N}$  a poor-ozone air tongue rises up to 11 km. This venting seems too strong and 11 km too high comparing to the ERA-40 reanalysis (see the

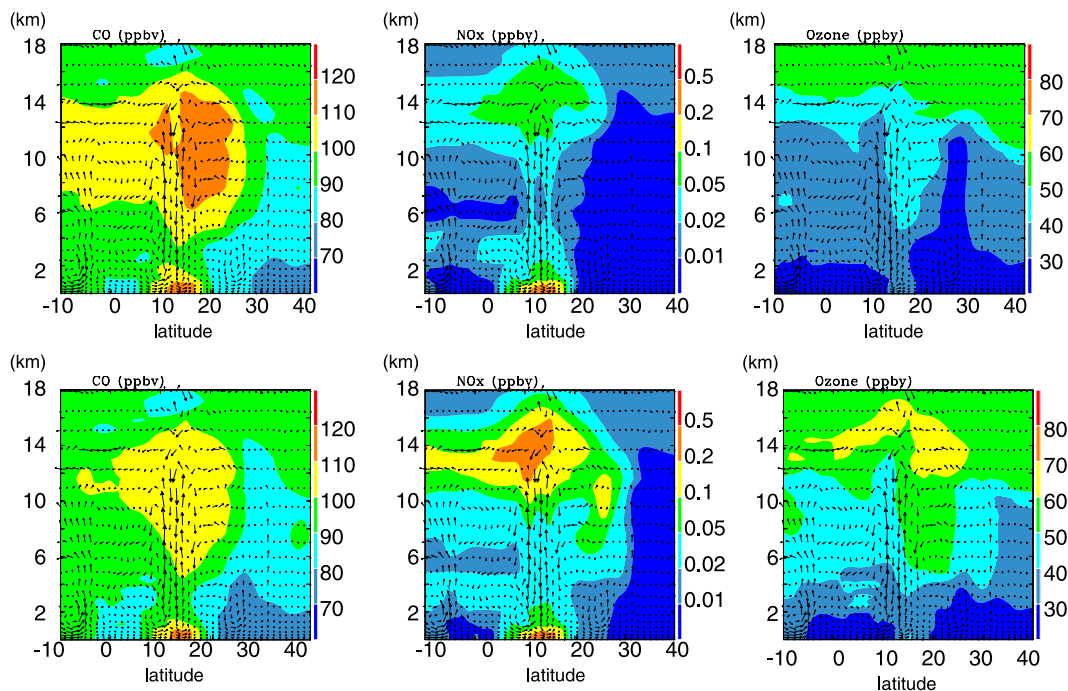


**Figure 3.** Vertical cross sections calculated for the 26th day of simulation at 1200 UTC: wind represented by vectors and  $\text{CO}$ ,  $\text{NO}_x$  and  $\text{O}_3$  mixing ratios in ppbv between  $-10^{\circ}\text{S}$  and  $40^{\circ}\text{N}$  for the two cases considered. Top: noLNOx case and bottom: LNOx case (see text for details).

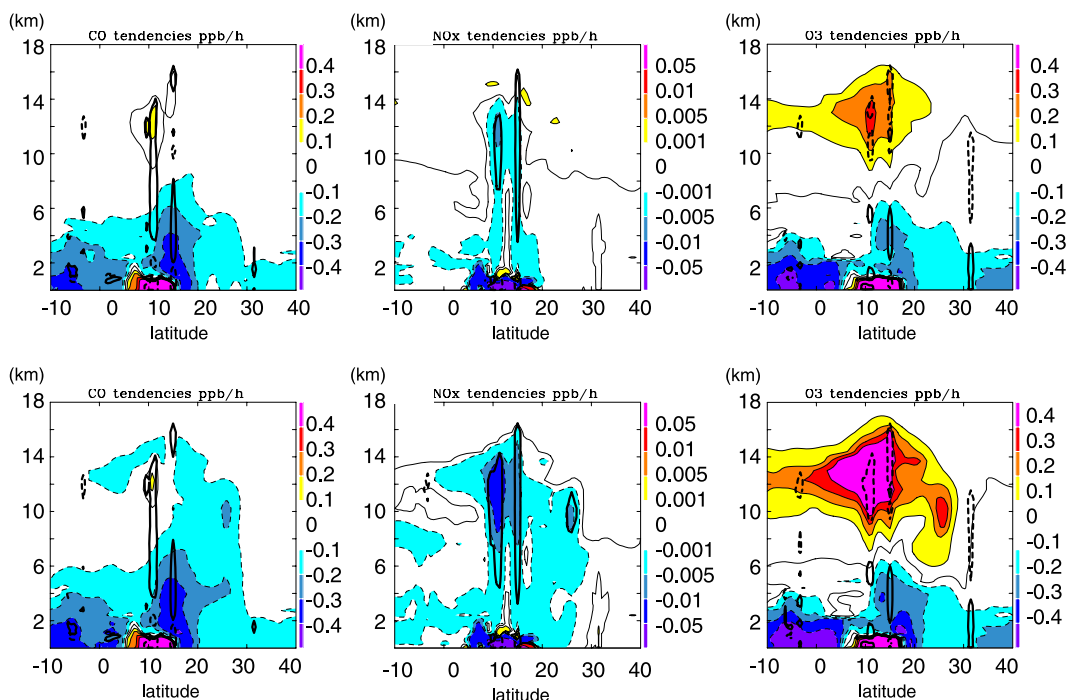


**Figure 4.** Vertical cross sections calculated for the 26th day of simulation at 1200 UTC: CO, NO<sub>x</sub> and O<sub>3</sub> tendencies in ppbv/h between  $-10^{\circ}$ S and  $40^{\circ}$ N for the two cases considered. Top: noLNOx case and bottom: LNOx case (see text for details). Convective tendency (thick lines) and chemical tendency (shaded). For the convective tendency, only the  $\pm 1$  ppbv/h isolines are shown for CO and O<sub>3</sub> and  $\pm 0.01$  ppbv/h for NO<sub>x</sub>.

differences on the vertical velocities in the Figures 4c and 5c by Peyrillé *et al.* [2007]). Feedback from the SubTropical Jet which could reduce the Heat Low intensity is probably missing in the model.

[20] Including LNOx leads to an important enhancement of NO<sub>x</sub> in the mid- and upper troposphere but almost none near the surface. The NO<sub>x</sub> maximum increases from  $\sim 0.1$  ppbv up to 0.3 ppbv at 14 km altitude between noLNOx and LNOx cases. The CO mixing ratios in Figure 3 decrease between noLNOx (top) and LNOx (bottom) simulations in the whole troposphere. A more intense oxidation of CO by an increased concentration of OH in the LNOx case leads to a loss of 5 to 15 ppbv of CO in the upper troposphere. In term of ozone chemistry, the decrease of CO is largely compensated by the large increase of NO<sub>x</sub>. The LNOx case shows an increase of 10–20 ppbv of O<sub>3</sub> in the mid- and upper troposphere. On the bottom right cross section in Figure 3, the convective transport of low O<sub>3</sub> air masses is also visible. It is interesting to note that the ITCZ corresponds to NO<sub>x</sub> maxima and O<sub>3</sub> minima. North and South of the ITCZ, O<sub>3</sub> maxima are simulated near the center of the cells where it seems to accumulate. The residence time of ozone increases in the middle of the northern cell because the vertical and meridional velocities almost reach zero. The extra ozone production compensates the impact of the low O<sub>3</sub> air masses in convective transport over the Heat Low in the LNOx case. At  $6^{\circ}$ S the convection is strong enough to create an ozone minimum and to trigger lightning and consequently to create a maximum of NO<sub>x</sub> at this latitude. However, the convection and associated LNOx source at  $6^{\circ}$ S are highly unlikely in the real world.

[21] The NO<sub>x</sub> values in the upper troposphere are weaker in the noLNOx case than in the LNOx case. We find a mixing ratio for NO<sub>y</sub>\* (not shown here, NO<sub>y</sub>\* = NO + NO<sub>2</sub> + HNO<sub>3</sub> + N<sub>2</sub>O<sub>5</sub> + PAN + NO<sub>3</sub>) around 0.3–0.4 ppbv for the noLNOx case and 0.6–0.7 ppbv for the LNOx case in the 9–12 km layer. The MOZAIC measurements during some flights over Africa showed that the NO<sub>y</sub> values range between 0.33 and 2.08 ppbv with a minimum at  $27^{\circ}$ N and a mean value of 0.94 ppbv over West Africa. Consequently the simulated NO<sub>y</sub> mixing ratios in the LNOx case are in the range of the observations. For the LNOx case, CO mixing ratios are around 90–110 ppbv and O<sub>3</sub> mixing ratios range between 40–70 ppbv near 9–12 km altitude.

## 5. Bidimensional Ozone Budget in the WAM System

[22] The convective and chemical tendencies have been extracted from the model to understand the redistribution of chemical species by the WAM system and quantify the ozone budget.

[23] The tendencies for the noLNOx case obtained the 26th day at 1200UTC are presented in Figure 4 (top). The convective tendencies are clearly collocated with the major ascents (around  $10^{\circ}$ N -ITCZ-,  $25^{\circ}$ N -Heat Low- and  $6^{\circ}$ S -over ocean-). Convection acts as a source for upper tropospheric CO and NO<sub>x</sub> with positive tendencies (higher than 1 ppbv/h for CO and 0.01 ppbv/h for NO<sub>x</sub>). On the contrary, convection brings poor O<sub>3</sub> air masses upward as shown by the negative tendencies in the upper troposphere (lower than  $-1$  ppbv/h). The chemical tendencies show a net production

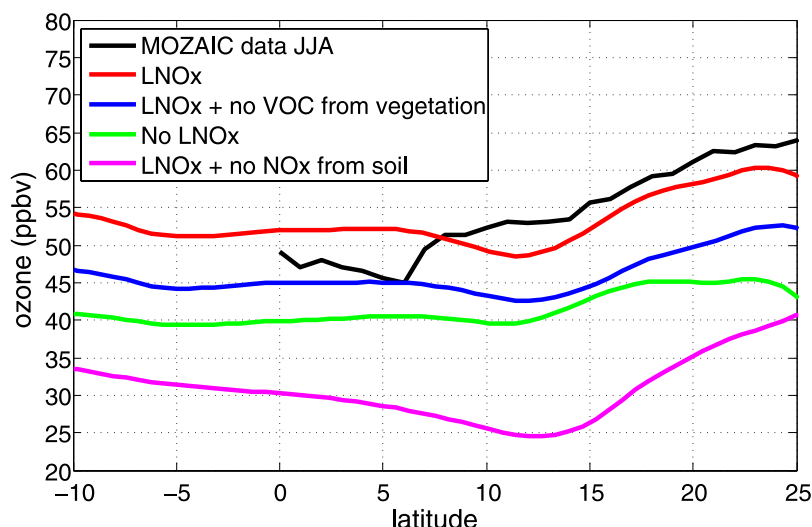


**Figure 5.** Meridional profiles of ozone in ppbv between  $-10^{\circ}\text{S}$  and  $25^{\circ}\text{N}$ . MOZAIC data and simulated ozone mixing ratios averaged between 9 and 12 km for the last five days for the four runs performed: LNOx, LNOx + no NOx from soils, LNOx + no VOCs and no LNOx.

of CO and  $\text{NO}_x$  in the boundary layer collocated with the natural emissions at the surface. The emitted precursors such as alkane, alkene, isoprene and terpene are vented into the upper troposphere where they are oxidized and produce CO above 10 km. Below 10 km altitude both CO and  $\text{NO}_x$  are oxidized by OH. Except very near the surface sources where ozone is produced, ozone is destroyed from the surface up to 8 km. In this region of the atmosphere concentrations of  $\text{NO}_x$  are very low ( $<50$  ppt) so  $\text{HO}_2$  reacts with  $\text{O}_3$  rather than with NO ( $\text{NO}_x$ -limited regime). Above 8 km, the net production of ozone is positive and around 0.1–0.2 ppbv/h where  $\text{NO}_x$  concentration is  $\sim 50$  ppt. These results agree well with the tropospheric ozone chemistry regimes described in the literature [Wennberg, 1998; Jaeglé *et al.*, 1999; Brune, 2000].

[24] The lightning source is counted together with the convective transport and so appears in the  $\text{NO}_x$  convective tendency. In the LNOx case, convection tendency for CO is comparable to the noLNOx case.  $\text{NO}_x$  convective tendencies are significantly increased by a factor of 3–4. The more spectacular change occurs for the  $\text{O}_3$  chemical tendencies which increase both in magnitude and expanse. The increase of  $\text{O}_3$  and  $\text{NO}_x$  in the Hadley cells leads to the increase of OH and to the subsequent loss of CO.

[25] A rough estimate of the 24 h change in ozone can be derived by calculating the 24 h average ozone chemical tendency. In the LNOx case, the 24h average ozone production stands around 0.25–0.30 ppbv/h downstream of the ITCZ. These values lead to a net change of 6–7 ppbv of ozone in 24h which has the same order of magnitude than those found by DeCaria *et al.* [2005] when the authors consider an average  $\text{NO}_x$  mixing ratios of 250–300 pptv. Using a chemistry-only version of a 3D cloud scale chemical transport model for the STEREO-A experiment they found ozone changes between 3–9 ppbv/day for  $\text{NO}_x$  mixing ratios of 250 pptv. Similarly, the impact of lightning  $\text{NO}_x$  can be inferred from the difference between simulations with and without this source. DeCaria *et al.* [2005]

found a difference in the ozone mixing ratios after 24 h in the range of 3–13 ppbv/day at 10.5 km. In this study, the 24 h-averaged difference in the ozone production rate with and without lightning reaches 5–6 ppbv/day.

## 6. Ozone Meridional Gradient in the WAM System

[26] On Figure 5 the ozone meridional gradient observed by MOZAIC is drawn with the averaged profiles of ozone between 9 and 12 km during the last 5 days of simulation for the four cases (LNOx, noLNOx, LNOx + no NOx soils, LNOx + no VOCs). Because no interaction with higher latitudes is allowed, the simulated profiles artificially converge toward the initial climatology values at  $40^{\circ}\text{N}$ . A sensitivity study shows that the ozone meridional profiles are influenced by the boundary conditions only north of  $24^{\circ}\text{N}$  (not shown). The northern ozone gradient which is calculated between  $12^{\circ}\text{N}$  and  $24^{\circ}\text{N}$  is unaffected by rigid boundary conditions. The NO produced by lightning increases the ozone concentration by 10–20 ppbv in the 9–12 km layer compared to the noLNOx case. The location of the minimum at the ITCZ is shifted to the North by about  $6^{\circ}$  compared to MOZAIC data. This is due to the northward drift of the convective region as discussed previously. The limits considered to calculate the ozone meridional gradients are the latitudes corresponding to the ozone profiles minima and maxima. The meridional gradients for the noLNOx are low (0.52 and 0.22 ppbv/deg respectively for the northern and the southern cells) compared to MOZAIC gradients (1.13 and 0.71 ppbv/deg). Adding the LNOx source increases the ozone gradient to 1.08 ppbv/deg in the northern cell and 0.60 ppbv/deg in the southern cell (Table 2). The ozone gradient are better reproduced when the LNOx source is active. The ozone gradient has more than doubled in the southern cell between noLNOx and LNOx cases, in better agreement with the observed gradient. Sensitivity simulations show that the ozone levels are



**Table 2.** Meridional Ozone Gradients Calculated on Both Sides of the ITCZ (North and South Cells) for the MOZAIC Data Analyzed in This Paper and by *Sauvage et al.* [2007b] and for the Simulations Performed With the 2D Model<sup>a</sup>

	Southern Cell		Northern Cell	
	Limits	Gradient	Limits	Gradient
MOZAIC data in this study	0°N–6°N	$-0.71 \pm 0.18$	7°N–32°N	$1.13 \pm 0.17$
MOZAIC data by <i>Sauvage et al.</i> [2007b]	19°S–5°N	$-0.62 \pm 0.09$	7°N–32°N	$0.94 \pm 0.18$
no LNO <sub>x</sub>	5.6°N–11.4°N	$-0.22 \pm 0.03$	11.4°N–23°N	$0.52 \pm 0.13$
LNO <sub>x</sub>	4.3°N–11.4°N	$-0.60 \pm 0.08$	11.4°N–23.7°N	$1.08 \pm 0.10$
LNO <sub>x</sub> + no NO <sub>x</sub> from soils	4°N–12.69°N	$-0.60 \pm 0.02$	12.69°N–24°N	$1.49 \pm 0.09$
LNO <sub>x</sub> + no VOCs from vegetation	4.9°N–12.0°N	$-0.41 \pm 0.05$	12.0°N–23.7°N	$0.95 \pm 0.05$

<sup>a</sup>The limits considered to calculate the gradients are given, the ozone gradient is in ppbv/deg.

sensitive to both surface and lightning emissions. The ozone mixing ratios are increased by 10–20 ppbv in the layer 9–12 km due to a photochemical production enhanced by additional NO<sub>x</sub> from lightning. The ozone change in the upper troposphere comes also partly from additional ozone at the surface when lightning source is active due to the downward convective mixing of rich ozone air masses produced in the upper troposphere [Lawrence *et al.*, 2003]. When the NO<sub>x</sub> source from soils is switched off (NO<sub>x</sub> only from lightning), ozone mixing ratio is dramatically decreased by about 20–25 ppbv in the upper troposphere. The ozone levels are also sensitive to the quantity of VOCs available in the UT. Interestingly, the ozone profiles in Figure 5 show that if the ozone levels (absolute values) are sensitive to the surface and lightning sources, the ozone gradients are only sensitive to the LNO<sub>x</sub> source. When the LNO<sub>x</sub> source is active, the ozone profiles have a well-marked northern gradient up to 24°N. This gradient flattens for latitudes north of 17°N without LNO<sub>x</sub>. On the southern branch, only the LNO<sub>x</sub> simulations exhibit an ozone meridional gradient providing that there is enough biogenic VOCs available. This result confirms the important role of the biogenic VOCs over Africa as proposed by *Aghedo et al.* [2007].

[27] Average ozone tendencies between 9 and 12 km are calculated for the LNO<sub>x</sub> case and presented in Figure 6

between 10°S and 25°N. The ozone convective tendency is negative and reaches  $-0.3$  ppbv/h at the ITCZ. The convective tendency at the ITCZ balances the intense photochemical production of ozone whereas (and particularly on the southern side) the convection is weaker and the chemical production dominates on both sides of the ITCZ. Thus the minimum of ozone is induced by the venting of O<sub>3</sub>-poor air masses from the boundary layer up to the upper troposphere similar to what is obtained over the oceanic regions [Folkins *et al.*, 2002; Mari *et al.*, 2003]. O<sub>3</sub>-poor air masses are also uplifted at 6°S leading to a secondary minimum of ozone in the upper troposphere which contributes to limit the southern gradient extent.

[28] Following *Sauvage et al.* [2007b], the ozone production rate can be derived from the ozone meridional advection assuming no vertical advection or convection within horizontal branches of the Hadley cells. The ozone meridional advection is derived by multiplying the ozone meridional gradient by the mean meridional wind in each cell. The values obtained are respectively 1.0 ppbv/day for the northern cell and 1.6 ppbv/day for the southern cell. These production rates are in the range of the rates derived from the MOZAIC observations by *Sauvage et al.* [2007b]. These values agree with the average rate derived from a higher resolution model by *DeCaria et al.* [2005] in cloud and non-

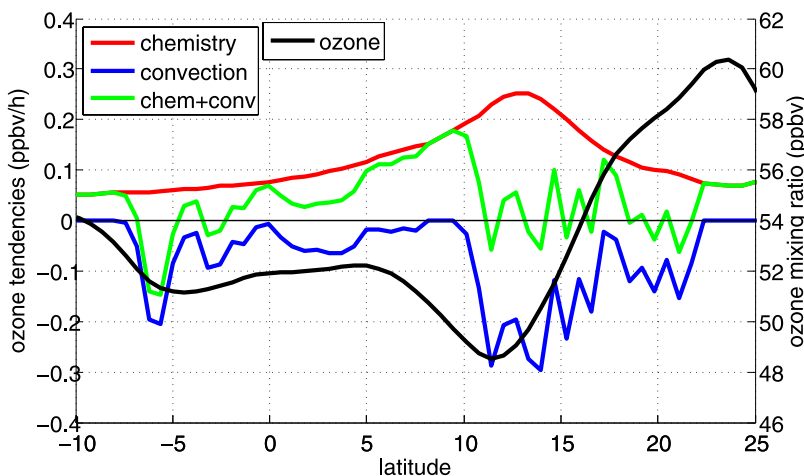


**Figure 6.** Meridional profiles of contributions to the ozone tendencies for the LNO<sub>x</sub> case in ppbv/h between  $-10^{\circ}$ S and  $25^{\circ}$ N: chemistry, convection and chemistry + convection contributions. The O<sub>3</sub> profile is plotted as well.

cloud influenced regions, 0.5–2 ppbv/day between 9 and 12 km altitude (see their Figure 12b).

## 7. Conclusion

[29] The aim of this work was to understand how the ozone meridional gradient observed by the MOZAIC measurements over West Africa could be induced. The study focused on the role of a meridional circulation corresponding to the Hadley cells. Thus a bidimensionnal version of the Méso-NH model is used to retrieve the main features of the West African monsoon dynamics and chemical signatures. A  $O_3$ - $NO_x$ -VOC chemical scheme has been added to the dynamical model together with surface emissions and a parametrization of the LNO<sub>x</sub> production.

[30] The model is able to reproduce the main features of the African Monsoon with the monsoon and the Harmattan fluxes on surface, the ITCZ around 10–15°N and the three main jets (African Easterly Jet, Tropical Easterly Jet and SubTropical Jet). However, the configuration of the model induces a northward drift of the ITCZ and the simulated northern Hadley cell is limited northward.

[31] Four simulations are presented in the paper. Among them, the simulation LNO<sub>x</sub> (noLNO<sub>x</sub>) considers all surface sources with (without) lightning NO<sub>x</sub> source. The ozone precursors emitted at the surface are uplifted by deep convection and then advected in the upper branches of the Hadley cells on both sides of the ITCZ. The maximum of ozone photochemical production is obtained near the ITCZ region but is compensated by the venting of poor ozone air masses from the boundary layer. This compensation induces the ozone minimum in the upper troposphere collocated with the ITCZ as observed in the MOZAIC data. Net ozone production is obtained in the Hadley cells with values between 2–4 ppbv/day. An ozone meridional gradient in the upper troposphere is recovered for all simulations which ranges from 0.22 to 0.52 ppbv/deg without the LNO<sub>x</sub> source and 0.60 to 1.08 ppbv/deg with the LNO<sub>x</sub> source, respectively in the southern and the northern Hadley cells. The bi-dimensional model suffers from limitations due to the absence of exchange with the higher latitudes and ventilation in the zonal direction. Despite of these restrictions, sensitivity simulations show that the LNO<sub>x</sub> source and biogenic VOCs are necessary to create the gradient in the southern Hadley cell. The LNO<sub>x</sub> source is also required to maintain the meridional ozone gradient up to 24°N in the northern Hadley cell.

[32] Additional work is now needed to assess the regional ozone budget over West Africa using three-dimensional models. In particular, the intrusion of biomass burning plumes from southern hemisphere *Sauvage et al.* [2005] and the westward flow from Asia should be considered to complete the picture of the ozone budget over West Africa. The measurements taken during the AMMA (African Monsoon Multidisciplinary Analysis) campaigns should help to better understand the sinks and sources of ozone over Africa.

[33] **Acknowledgments.** The authors acknowledge MOZAIC funding agencies, the European Commission, CNRS (France), Forschungszentrum Jülich (Germany), Météo France, EADS (Airbus) and the airlines (Air France, Lufthansa, Austrian Airlines and former Sabena) who carry free of charge the MOZAIC equipment and perform the maintenance. The emis-

sions values are taken from the GEIA-ACCENT database, an international cooperative activity of AIMES/IGBP, sponsored by the ACCENT EU Network of Excellence. Computer time has been provided by the Institut du Développement et des Ressources en Informatique Scientifique (IDRIS). On the basis of a French initiative, AMMA was built by an international scientific group and is currently funded by a large number of agencies, especially from France, the United Kingdom, the United States, and Africa. It has been the beneficiary of a major financial contribution from the European Communities Sixth Framework Research Programme. Detailed information on scientific coordination and funding is available on the AMMA International Web site at [www.amma-international.org](http://www.amma-international.org). The authors would like to thank the anonymous reviewers for their thoughtful comments.

## References

- Aghedo, A., M. Shultz, and S. Rast (2007), The influence of African air pollution on regional and global tropospheric ozone, *Atmos. Chem. Phys.*, **7**, 1193–1212.
- Bechtold, P., E. Bazile, F. Guichard, P. Mascart, and E. Richard (2001), A mass-flux convection scheme for regional and global models, *Q. J. R. Meteorol. Soc.*, **127**, 869–886.
- Bond, D. W., S. Steiger, R. Zhang, X. Tie, and R. Orville (2002), The importance of NO<sub>x</sub> production by lightning in the tropics, *Atmos. Environ.*, **36**.
- Bougeault, P., and P. Lacarrère (1989), Parametrization of orography induced turbulence in a mesobeta-scale model, *Mon. Weather Rev.*, **117**, 1872–1890.
- Brune, W. (2000), OH and HO<sub>2</sub>: Sources, interactions with nitrogen oxides and ozone production, *Global Change Newslett.*, **43**, 5255–5270.
- Chou, C., J. Neelin, and H. Su (2001), Ocean-atmosphere-land feedbacks in an idealized monsoon, *Q. J. R. Meteorol. Soc.*, **127**(576), 1869–1891.
- Christian, H., et al. (2003), Global frequency and distribution of lightning as observed by the optical transient detector, *J. Geophys. Res.*, **108**(D1), 4005, doi:10.1029/2002JD002347.
- Crassier, V., K. Shure, P. Tulet, and R. Rosset (2000), Development of a reduced chemical scheme for use in mesoscale meteorological models, *Atmos. Environ.*, **34**, 2633–2644.
- Cuxart, J., P. Bougeault, and J.-L. Redelsperger (2000), A turbulence scheme allowing for mesoscale and large-eddy simulations, *Q. J. R. Meteorol. Soc.*, **126**, 1–30.
- DeCaria, A., K. Pickering, G. Stenchikov, and L. Ott (2005), Lightning-generated NO<sub>x</sub> and its impact on tropospheric ozone production: A three dimensional modeling study of a Stratosphere-Troposphere Experiment: Radiation, Aerosols and Ozone (STERAO-A) thunderstorm, *J. Geophys. Res.*, **110**, D14303, doi:10.1029/2004JD005556.
- Douville, H., S. Conil, S. Tyteca, and A. Voltaire (2007), Soil moisture memory and West African monsoon predictability: Artefact or reality?, *Clim. Dyn.*, **28**, 723–742.
- Edwards, D. P., et al. (2006), Satellite observed pollution from southern hemisphere biomass burning, *J. Geophys. Res.*, **111**, D14312, doi:10.1029/2005JD006655.
- Eltahir, E., and C. Gong (1996), Dynamics of wet and dry years in West Africa, *J. Clim.*, **9**, 1030–1042.
- Folkens, I., C. Braun, A. Thompson, and J. Witte (2002), Tropical ozone as an indicator of deep convection, *J. Geophys. Res.*, **107**(D13), 4184, doi:10.1029/2001JD001178.
- Giannini, A., R. Saravanan, and P. Chang (2003), Oceanic forcing of Sahel rainfall on interannual to interdecadal time scales, *Science*, **302**, 1027–1030.
- Guenther, C. N., et al. (1995), A global model of natural volatile organic compound emissions, *J. Geophys. Res.*, **100**(D5), 8873–8892.
- Guenther, A., T. Karl, C. Wiedinmyer, P. Palmer, and C. Geron (2006), Estimates of global terrestrial isoprene emissions using MEGAN (Model of Emissions of Gases and Aerosols from Nature), *Atmos. Chem. Phys.*, **6**, 3181–3210.
- Helten, M., H. Smit, W. Straäter, D. Kley, P. Nédélec, M. Zöger, and R. Busen (1998), Calibration and performance of automatic compact instrumentation for the measurement of relative humidity from passenger aircraft, *J. Geophys. Res.*, **103**(D19).
- Jaeglé, L., et al. (1999), Ozone production in the upper troposphere and the influence of aircraft during SONEX: Approach of NO<sub>x</sub>-saturated conditions, *Geophys. Res. Lett.*, **26**, 3081–3084.
- Jaeglé, L., et al. (2004), Satellite mapping of rain-induced nitric oxide emissions from soils, *J. Geophys. Res.*, **109**, D21310, doi:10.1029/2004JD004787.
- Jaeglé, L., L. Steinberger, R. Martin, and K. Chance (2005), Global partitioning of NO<sub>x</sub> sources using satellite observations: Relative roles of fossil fuel combustion, biomass burning and soils emissions, *Faraday Discuss.*, **130**, 1–17.

- Jonquière, I., A. Marengo, A. Maalej, and F. Rohrer (1998), Study of ozone formation and transatlantic transport from biomass burning emissions over West Africa during the airborne Tropospheric Ozone Campaigns TROPOZ I and TROPOZ II, *J. Geophys. Res.*, *103*(D15), 19,059–19,073.
- Labrador, L., R. von Kuhlmann, and M. Lawrence (2005), The effects of lightning-produced NO<sub>x</sub> and its vertical distribution on atmospheric chemistry: Sensitivity simulations with MATCH-MPIC, *Atmos. Chem. Phys.*, *5*, 1815–1834.
- Lafore, J.-P., et al. (1998), The Meso-NH atmospheric simulation system. Part I: Adiabatic formulation and control simulations, *Ann. Geophys.*, *16*, 90–109.
- Lawrence, M., R. von Kuhlmann, and M. Salzmann (2003), The balance of effects of deep convective mixing on tropospheric ozone, *Geophys. Res. Lett.*, *30*(18), 1940, doi:10.1029/2003GL017644.
- Mahfouf, J.-F., and J. Noilhan (1996), Inclusion of gravitational drainage in a land surface scheme based on the forced-restore method, *J. Appl. Meteorol.*, *35*, 987–992.
- Marengo, A., et al. (1998), Measurement of ozone and water vapor by airbus in-service aircraft: The MOZAIC airborne program, an overview, *J. Geophys. Res.*, *103*(D19), 25,631–25,642.
- Mari, C., D. Jacob, and P. Bechtold (2000), Transport and scavenging of soluble gases in deep convection cloud, *J. Geophys. Res.*, *105*(D17), 22,255–22,267.
- Mari, C., et al. (2003), On the relative role of convection, chemistry and transport over the South Pacific Convergence Zone during PEM-Tropics B: A case study, *J. Geophys. Res.*, *108*(D2), 8232, doi:10.1029/2001JD001466.
- Mari, C., et al. (2006), Regional lightning NO<sub>x</sub> sources during the TROC-CINOX experiment, *Atmos. Chem. Phys.*, *6*, 5559–5572.
- Martin, R., D. Jacob, J. Logan, J. Ziemke, and R. Washington (2000), Detection of a lightning influence on tropical tropospheric ozone, *Geophys. Res. Lett.*, *27*(11).
- Martin, R. V., B. Sauvage, I. Folkens, C. E. Sioris, C. Boone, P. Bernath, and J. Ziemke (2007), Space-based constraints on the production of nitric oxide by lightning, *J. Geophys. Res.*, *112*, D09309, doi:10.1029/2006JD007831.
- Mondon, S., and J.-L. Redelsperger (1998), A study of a fair weather boundary layer in togacoare: Parametrization of surface fluxes in large scale and regional models for light wind conditions, *Boundary Layer Meteorol.*, *88*, 47–76.
- Olivier, J., J. Peters, C. Granier, G. Petron, J. Müller, and S. Wallens (2003), Present and future surface emissions of atmospheric compounds, *Poet report nr. 2*, EU project EVK2-1999-0001.
- Pätz, H., A. Volz-Thomas, M. Hegglin, D. Brunner, H. Fischer, and U. Schmidt (2006), In-situ comparison of the NO<sub>y</sub> instruments flown in MOZAIC and SPURT, *Atmos. Chem. Phys.*, *6*, 2401–2410.
- Peyrillé, P., J.-P. Lafore, and J.-L. Redelsperger (2007), An idealized two-dimensional framework to study the West African monsoon, Part I: Validation and key controlling factors, *J. Atmos. Sci.*, *64*(8), 2765–2782.
- Peyrillé, P., and J.-P. Lafore (2007), An idealized two-dimensional framework to study the West African monsoon, Part II: Large scale advection and the diurnal cycle, *J. Atmos. Sci.*, *64*(8), 2783–2803.
- Pickering, K. E., et al. (1996), Convective transport of biomass burning emissions over Brazil during TRACE A, *J. Geophys. Res.*, *101*(D19), 23,993–24,012.
- Pinker, R. T., Y. Zhao, C. Akoshile, J. Janowiak, and P. Arkin (2006), Diurnal and seasonal variability of rainfall in the sub-Sahel as seen from observations, satellites and a numerical model, *Geophys. Res. Lett.*, *33*, L07806, doi:10.1029/2005GL025192.
- Price, C., and D. Rind (1992), A simple lightning parametrization for calculating global lightning distributions, *J. Geophys. Res.*, *97*, 9919–9933.
- Price, C., and D. Rind (1993), What determines the cloud-to-ground lightning fraction in thunderstorm?, *J. Geophys. Res.*, *20*(6), 463–466.
- Redelsperger, J.-L., A. Diongue, A. Diedhou, J.-P. Cero, M. Diop, J.-F. Gueremy, and J.-P. Lafore (2002), Multi-scale description of a Sahelian synoptic weather system representative of the West African monsoon, *Mon. Weather Rev.*, *130*, 1229–1257.
- Reynolds, R., and W. Smith (1995), A high-resolution global sea surface temperatures climatology, *J. Clim.*, *8*, 1571–1583.
- Rowell, D., C. Folland, K. Maskell, and M. Ward (1995), Variability of summer rainfall over tropical North Africa, *Q. J. R. Meteorol. Soc.*, *121*, 669–704.
- Sauvage, B., V. Thouret, J.-P. Cammas, F. Gheusi, G. Athier, and P. Nédélec (2005), Tropospheric ozone over Equatorial Africa: Regional aspects from the MOZAIC data, *Atmos. Chem. Phys.*, *5*, 311–335.
- Sauvage, B., R. V. Martin, A. van Donkelaar, and J. R. Ziemke (2007a), Quantification of the factors controlling tropical tropospheric ozone and the South Atlantic maximum, *J. Geophys. Res.*, *112*, D11309, doi:10.1029/2006JD008008.
- Sauvage, B., V. Thouret, J.-P. Cammas, J. Brioude, P. Nédélec, and C. Mari (2007b), Meridional ozone gradients in the African upper troposphere, *Geophys. Res. Lett.*, *34*, L03187, doi:10.1029/2006GL028542.
- Seinfeld, J., and S. Pandis (1998), *Atmospheric Chemistry and Physics: From Air Pollution to Climate Change*, John Wiley and Sons.
- Serça, D., R. Delmas, X. Le Roux, D. A. B. Parsons, M. C. Scholes, L. Abbadie, R. Lensi, O. Ronce, and L. Labroue (1998), Comparison of nitrogen monoxide emissions from several African tropical ecosystems and influence of season and fire, *Global Biogeochem. Cycles*, *12*(04).
- Simmons, A., and J. Gibson (2000), The ERA40 Project Plan. ERA-40 project report series No. 1, ECMWF, Shinfield Park, Reading, United Kingdom, 63 pp.
- Stockwell, W., F. Kirchner, M. Kuhn, and S. Seefeld (1997), A new mechanism for regional atmospheric chemistry modeling, *J. Geophys. Res.*, *102*, 25,847–25,879.
- Thiaw, W. M., and K. C. Mo (2005), Impact of sea surface temperature and soil moisture on seasonal rainfall prediction over the Sahel, *J. Clim.*, *18*(24), 5330–5343.
- Thompson, A. M. (1992), The oxidizing capacity of the Earth's atmosphere: Probable past and future changes, *Science*, *256*, 1157–1165.
- Thouret, V., A. Marengo, J. Logan, P. Nédélec, and C. Grouhel (1998a), Comparisons of ozone measurements from the MOZAIC airborne program and the ozone sounding network at eight locations, *J. Geophys. Res.*, *103*(D19).
- Thouret, V., A. Marengo, P. Nédélec, and C. Grouhel (1998b), Ozone climatologies at 9–12 km altitude as seen by MOZAIC airborne program between September 1994 and August 1996, *J. Geophys. Res.*, *103*(D19), 25,653–25,680.
- Volz-Thomas, A., M. Berg, T. Heil, N. Houben, A. Lerner, W. Petrick, D. Raak, and H. W. Ptz (2005), Measurements of total odd nitrogen (NO<sub>y</sub>) aboard MOZAIC in-service aircraft: Instrument design, operation and performance, *Atmos. Chem. Phys.*, *5*, 583–595.
- von Kuhlmann, R., and M. Lawrence (2006), The impact of ice uptake of nitric acid an atmospheric chemistry, *Atmos. Chem. Phys.*, *6*, 225–235.
- von Kuhlmann, R., M. Lawrence, P. Crutzen, and P. Rasch (2003), A model for studies of tropospheric ozone and non-methane hydrocarbons: Model description and ozone results, *J. Geophys. Res.*, *108*(D9), 4294, doi:10.1029/2002JD002893.
- Wang, G., and E. Eltahir (2000), Biosphere-atmosphere interactions over West Africa. II: Multiple climate equilibria, *Q. J. R. Meteorol. Soc.*, *126*, 1261–1280.
- Wennberg, P. (1998), Hydrogen radicals, nitrogen radicals and the production of ozone in the middle and upper troposphere, *Science*, *279*, 49–53.
- Zeng, N., J. Neelin, K.-M. Lau, and J. Compton (1999), Enhancement of interdecadal climate variability in the Sahel by vegetation interaction, *Science*, *286*, 1537–1540.
- Zheng, X., E. A. B. Eltahir, and K. A. Emmanuel (1999), A mechanism relating tropical Atlantic sea surface temperature and west African rainfall, *Q. J. R. Meteorol. Soc.*, *125*, 1129–1163.

J. P. Cammas, C. Mari, P. Nédélec, J. P. Pinty, M. Saunois, B. Sauvage, and V. Thouret, Université de Toulouse, Laboratoire d'Aérodynamique, OMP, 14 avenue E. Belin, Toulouse, 31 500, France. (marielle.saunois@aero.obs-mip.fr)

J. P. Lafore and P. Peyrillé, Centre National de Recherches Météorologiques, Toulouse, France.

A. Volz-Thomas, Institut für Chemie und Dynamik der Geosphäre II: Troposphäre, Forschungszentrum Jülich, Jülich, Germany.